

Restoring Images Captured in Arbitrary Hybrid Adverse Weather Conditions in One Go

Yecong Wan

China University of Petroleum (East China)
yecongwan@gmail.com

Yuanshuo Cheng

China University of Petroleum (East China)

Mingwen Shao

China University of Petroleum (East China)

Yuexian Liu

China University of Petroleum (East China)

Zhiyuan Bao

China University of Petroleum (East China)

Abstract

Adverse conditions typically suffer from stochastic hybrid weather degradations (e.g., rainy and hazy night), while existing image restoration algorithms envisage that weather degradations occur independently, thus may fail to handle real-world complicated scenarios. Besides, supervised training is not feasible due to the lack of a comprehensive paired dataset to characterize hybrid conditions. To this end, we have advanced the aforementioned limitations with two tactics: framework and data. First, we present a novel unified framework, dubbed RAHC, to Restore Arbitrary Hybrid adverse weather Conditions in one go. Specifically, our RAHC leverages a multi-head aggregation architecture to learn multiple degradation representation subspaces and then constrains the network to flexibly handle multiple hybrid adverse weather in a unified paradigm through a discrimination mechanism in the output space. Furthermore, we devise a reconstruction vectors aided scheme to provide auxiliary visual content cues for reconstruction, thus can comfortably cope with hybrid scenarios with insufficient remaining image constituents. Second, we construct a new dataset, termed HAC, for learning and benchmarking arbitrary Hybrid Adverse Conditions restoration. HAC contains 31 scenarios composed of an arbitrary combination of five common weather, with a total of $\sim 316K$ adverse-weather/clean pairs. Extensive experiments yield superior results and establish new state-of-the-art results on both HAC and conventional datasets.

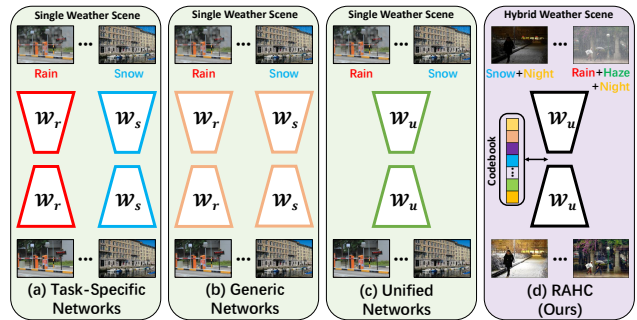


Figure 1. **Overview of adverse conditions restoration frameworks.** (a) Separate networks designed for specific tasks; (b) generic networks with task-specific weights; (c) unified all-in-one networks with single trained weights; (d) our proposed RAHC framework. In contrast to existing approaches that aim to tackle conditions with a single weather type, RAHC can handle arbitrary hybrid adverse weather conditions in one go, thus enjoying better flexibility and practicality in practical applications.

1. Introduction

In real-world adverse scenarios, different weather degradations often occur simultaneously in an uncertain way, e.g., snowy night, rainy night. Images captured under these conditions inevitably suffer abysmal visibility and corrupted feature remnants, and the stochastic hybrid degradation may dramatically hamper high-level vision tasks [3, 6, 9, 32] in applications such as autonomous driving systems [27, 39, 40] and surveillance systems [38]. Unfortunately, prevalent algorithms [71, 29, 68, 44] deal with each weather degradation individually ignoring the hybrid degradation characterization of combined action. Specifically, early researchers focused on developing task-specific

restoration algorithms for given weather conditions [7, 41, 10, 54, 28] (Fig. 1(a)). Afterwards various generic networks were proposed to handle different degradations with identical architecture [65, 4, 26, 56] (Fig. 1(b)), but with different weights for different tasks. To address this issue, recent researches aim at restoring images under multiple adverse conditions with a single unified model [8, 25, 22, 50] (Fig. 1(c)). Nevertheless, these methods still fail to address hybrid adverse weather conditions. Despite few works [24, 43, 53] have partly explored restoring two-weather superimposed scenarios, they were designed for specialized combinations (e.g., rain streak and raindrop) and could not extend to other real-world diverse hybrid scenarios.

To more flexibly and practically deal with real-world scenarios, a turnkey solution that can restore arbitrary hybrid adverse conditions in one go is urgently needed. Compared to this goal, the existing works have the following limitations. (i) Existing restoration networks are limited in characterizing hybrid multiple weather degradations simultaneously due to the lack of a multi-subspace feature extraction mechanism. (ii) Models utilized in single degradation removal are restricted in restoring hybrid adverse weather conditions with insufficient remaining background constituents. (iii) Previous unified learning strategies are designed for non-overlapping degradations and are constrained to popularize to diverse hybrid scenarios.

To tackle the aforementioned problems, in this paper, we propose a novel unified framework RAHC to restore arbitrary hybrid adverse weather conditions in one go (Fig. 1(d)). Specifically, we present three tailored designs to overcome the above limitations. (i) Multi-head blend block (MHBB) for multi-weather degradation representation: the multi-head mechanism overriding the blend operator of convolution and attention can provide multiple “representation subspaces” [52] as well as complementary features for hybrid multi-weather learning. (ii) Reconstruction vectors aided restoration (RVA) for hybrid conditions with limited image constituents retention: the discrete representations encapsulated in the Codebook [11] pre-trained on large-scale natural images which we refer to as reconstruction vectors, can provide additional visual content cues to auxiliary the reconstruction of realistic and clean output. (iii) Output space discrimination (OSD) for efficient arbitrary hybrid conditions restoration: we design a simple multilabel-classification discriminator from the output space to force the restoration network to learn degradation-independent repair capabilities which can flexibly cope with diverse hybrid scenarios without any complex strategies or modules. Especially noteworthy is that this protocol can be seamlessly integrated into existing universal image restoration algorithms boosting their performance in the all-in-one multi-weather removal setting.

Apart from the network, we manage to construct a hy-

brid adverse weather conditions dataset HAC, which covers $\sim 316K$ pairs of $2^5 - 1 = 31$ adverse conditions with five common weather types (namely haze, rain streak, snow, night, and raindrop) arranged in combination except for the clean one. To synthesize sufficient and diverse pairwise data efficiently and at low consumption, we develop a powerful generator AdverseGAN to learn from adverse conditions so as to approximate the degradation implicitly rather than expensive manual labeling. Thus, the training set can be automatically generated by AdverseGAN with minimal labor cost. To guarantee authoritative evaluation, the test set is meticulously handcrafted by our recruited experts. The domain gap between the training and test sets allows for better evaluation of the generalization ability which is critical for real-world applications, especially when the real data is infeasible. Comprehensive experimental results substantiate the superiority of the RAHC beyond state-of-the-art restoration methods on both HAC and conventional datasets.

In conclusion, the main contributions are summarized as follows:

- We propose a novel framework, dubbed RAHC, to restore diverse hybrid adverse weather conditions while enjoying the properties of being concise, flexible, and powerful.
- We present a multi-head blend block to provide multiple representation subspaces for multi-degeneration learning. Meanwhile, a reconstruction vectors aided restoration scheme is devised for severely deteriorated hybrid adverse conditions, as well as an output space discrimination regime for unified learning of diverse hybrid degradations.
- A new synthetic dataset HAC for arbitrary hybrid adverse weather conditions restoration is constructed. To the best of our knowledge, HAC is the first to encompass such a wide range of scenarios and provides the most comprehensive benchmark for this task.
- Extensive experimental results on HAC and conventional datasets demonstrate the effectiveness, superiority, and robustness of our proposed RAHC.

2. Related Work

2.1. Adverse Weather Conditions Restoration

Numerous algorithms have been proposed to recover images captured in adverse weather conditions, e.g., rain [54, 13], haze [42, 59, 48], snow [30, 7], etc. While these methods perform well on the specific weather type, significant performance degradation was observed when migrating to other tasks. Aiming at this limitation, a broad spectrum of research [66, 67, 65, 5, 4] has explored generic frameworks to accommodate different degradation types with an identical network. Even so, they still require separate training of independent weights for each task, hinder-

ing its generalizability. To repair multiple degradations in an all-in-one fashion, several unified models are proposed [8, 25, 22, 50]. However, these approaches ignore that real-world adverse conditions often suffer from superimposed multiple degradations [24], e.g., rain streaks and raindrops [43], rain and nighttime [53], etc. In this paper, adverse scenarios with an arbitrary hybrid of five weather types are considered for a total of 31 conditions, and RAHC can cope with all conditions in one go driving arbitrary hybrid adverse conditions restoration in a broad sense.

2.2. Pseudo Data Generation

Data-driven vision tasks rely heavily on high-quality datasets. Unfortunately, the labeling and acquiring of data tends to be expensive, challenging and time-consuming. To surmount this bottleneck, several recent efforts [70, 62, 55, 31] delve into pseudo-data generation by leveraging Generative Adversarial Networks (GAN). For instance, Zhang *et al.* [70] proposed a DatasetGAN to synthesize highly realistic images with pixel-wise annotations, the model trained on the synthetic dataset can even surpass the ones trained on the real dataset. Yang *et al.* [62] released SurfGAN, which facilitates the training of autonomous driving models by simulating realistic road scenarios. In addition to high-level tasks, this research boom has also been conveyed to low-level tasks. Wang *et al.* [55] exceeded SOTA with only 0.17% original data and synthesized pseudo-data. Yue *et al.* [64] introduced a dual adversarial network to simultaneously tackle noise removal and noise generation. Inspired by CycleGAN [72], Wei *et al.* [58] generated a pseudo-paired dataset Rain200A by cycle translation, and the models trained on it exhibit better robustness and generalization. Inspired by these pioneer works, we pursue the efficient and inexpensive synthesis of paired data for training by utilizing a deliberate GAN.

2.3. Perceptual Image Compression

Tremendous success in two-stage image generation [11, 61, 63, 45, 46] based on perceptual image compression has been witnessed. These works compress images into discrete latent vectors in the first stage and synthesize high-quality images leveraging encoded vectors in the second stage. In this paper, we focus on perceptual image compression in the first stage. VQVAE [45] first presents an auto-encoder model to implement multi-scale quantization of images. Based on VQVAE, VQGAN [11] introduces adversarial and perceptual objectives to obtain higher compression rates while preserving satisfactory perceptual quality. Furthermore, LDM [46] explores different compression rates and different kinds of regularizations, deriving a compression model that is more adept at preserving details. Intrigued by the extensive image priors contained in the discrete latent vectors of image compression, we advocate utilizing these auxiliary priors to guide the restoration, since

the discrete vector comprises context-rich visual parts.

2.4. Unsupervised Domain Adaptation (UDA)

UDA algorithms [15, 17, 35, 49, 33, 34, 73] for semantic segmentation aim to constrain the model trained on the source domain to learn domain-invariant features, thereby generalizing to the target domain. One category of these studies [49, 33, 34, 73] was devoted to training a discriminator to distinguish whether the output results come from the source or target domain, while the segmentation network learns domain-invariant knowledge to confuse the discriminator. Motivated by these methods, RAHC interestingly treats the uniform restoration of different degradations as a domain adaptive problem, as will be demonstrated, fooling a degradation type classifier is more straightforward and concise than sophisticated units and training strategies in degradation-independent feature learning.

3. Methodology

3.1. Overview of the Proposed Method

The training procedure for RAHC is illustrated in Fig. 2. RAHC aims to tackle arbitrary hybrid adverse conditions restoration via a unified framework, and the central notion is to efficiently generate hybrid adverse scenarios by AdverseGAN and then train a degeneration-independent restoration network through multi-head aggregation structure and discriminative learning scheme. Simultaneously, the visual constituents embedded in the Codebook are leveraged to provide auxiliary visual cues for the restoration of highly difficult hybrid conditions. Formally, given a clean image $C \in \mathbb{R}^{H \times W \times 3}$, AdverseGAN first generates the corresponding degraded ones $D \in \mathbb{R}^{H \times W \times 3}$ to obtain the degraded-clean pair. The generated degraded image is then fed into the restoration network to produce the consistent restoration-independent restored image $R \in \mathbb{R}^{H \times W \times 3}$. Meanwhile, the feature mapping network learns the projection from the encoded feature to corresponding clean embedding to locate the reconstruction vectors in the Codebook, supplying additional auxiliary visual atoms for restoration. Finally, the restored result is input into the discriminator to distinguish which type of degradation the restored image suffered before the restoration. The whole procedure is a snap, and there is no extra inference cost or modification during testing besides the restoration network.

3.2. Network Architecture

The restoration network adheres to a U-shaped structure, which hierarchically cascades multiple tailored multi-head blend blocks, and the knowledge domain is broadened at the bottleneck supported by reconstruction vectors, thereby leading to more optimal repair results. Mathematically, given a degraded image $D \in \mathbb{R}^{H \times W \times 3}$, a 3×3 convolution is first adopted to produce shallow feature embed-

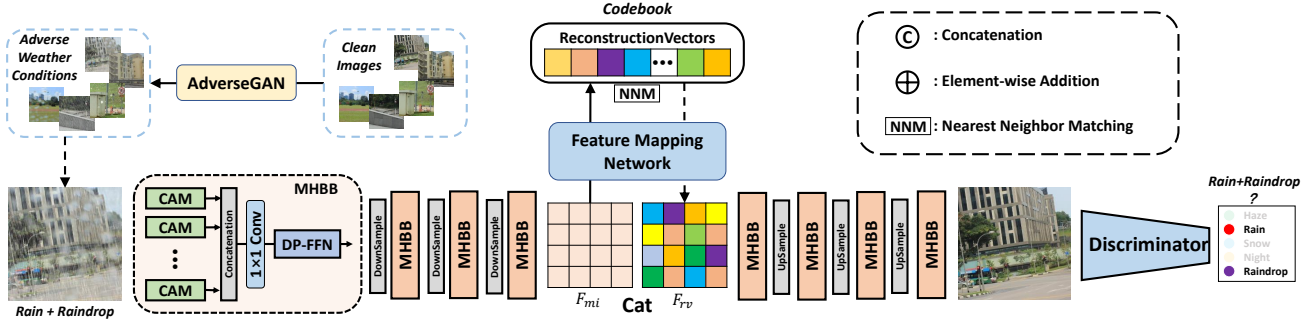


Figure 2. Illustration of the proposed RAHC architecture. The restoration network consists of an encoder, a decoder, and a feature mapping subnetwork. The mapping network first maps the encoded feature to the latent clean space and then locates the reconstruction vectors in the pre-established Codebook by nearest neighbor matching to provide privileged visual cues for the decoder. To enable degradation-independent learning, we utilize a discriminator to distinguish the type of weather degradation from the restored image while the restoration network struggles to fool the discriminator.

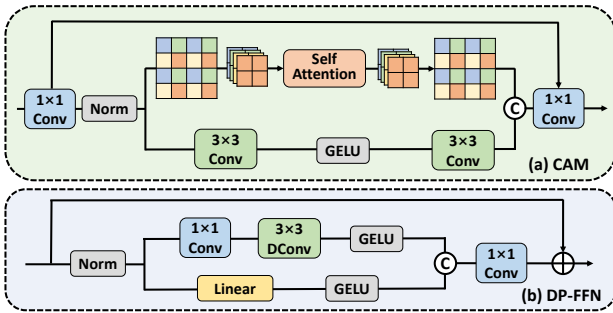


Figure 3. (a) Schematic diagrams for Convolution-Attention Module (CAM); (b) Dual-Path Feed-Forward Network (DP-FFN).

dings $F_{in} \in \mathbb{R}^{H \times W \times C}$. Then, F_{in} is propagated through four encoder layers built upon MHBB to obtain the deep feature $F_{mi} \in \mathbb{R}^{\frac{H}{8} \times \frac{W}{8} \times 8C}$. Thereafter, F_{mi} is transmitted by the feature mapping network to locate the reconstruction vectors $F_{rv} \in \mathbb{R}^{\frac{H}{8} \times \frac{W}{8} \times N_z}$ that most likely can reconstruct the hidden clean image from the Codebook, where N_z represents the dimension of reconstruction vector. Eventually, F_{mi} and F_{rv} are concatenated together and fed into the symmetric decoder to recover the final result $R \in \mathbb{R}^{H \times W \times 3}$ via a 3×3 convolution. Next, we will describe the core components of the proposed restoration network.

Multi-Head Blend Block (MHBB). Existing feature extraction modules lack a multi-degradation representation mechanism to capture the characteristics of hybrid multiple weather, leading to inadequate feature modeling. Besides, the complementary properties of convolution, which has strong local computational capabilities, and Transformer, which is excellent at capturing long-range dependencies, make the hybrid structure a better alternative for feature extraction [69, 14]. To this end, we propose a Multi-Head Blend Block (MHBB) to provide multiple “representation subspaces” as well as complementary features for multi-weather learning. Fig. 3 illustrates the two core units (CAM & DP-FFN) of MHBB. Instead of combining Transformer and Convolution directly in parallel or series, we treat con-

volution and self-attention as equivalent micro-level operators. And the multi-head mechanism overriding multiple CAMs can provide multi-degradation representation subspaces for unified learning. To be specific, an input feature X , is first divided into “heads” which bears a resemblance to the vanilla Transformer [52]. The multi-head design allows separate branches to learn different representations and thus adaptively extract different degradation cues to guarantee the ability of diversity restoration. Each head is then transformed by a Convolution-Attention Module (CAM). CAM contains two branches: the attention path and the convolution path, which are split and merged for parallel processing with the addition of 1×1 convolution. To reduce the high computational effort of vanilla self-attention while preserving the global computational properties, we adopt the pixel-shuffle [47] operator in the attention path to diminish the number of tokens while avoiding information loss. The convolution path, on the other hand, consists of two convolutional layers and a GELU activation function. Then, the results of different heads are integrated together with a 1×1 convolutional stacked subsequently. Locally relevant information is crucial for image restoration, while the original Feed-Forward Network (FFN) is insensitive and inept at this demand. To compensate for the limitations, we invent a Dual-Path FFN (DP-FFN) to extract local contextual information by introducing convolutional branches parallel with a fully connected layer. Overall, the MHBB process can be expressed as:

$$\hat{Y} = \text{Cat}(\text{CAM}_1(X_1), \text{CAM}_2(X_2), \dots, \text{CAM}_k(X_k)), \quad (1)$$

$$Y = \text{DP-FFN}(\text{Conv}1 \times 1(\hat{Y})).$$

Reconstruction Vectors Aided Restoration. Existing image restoration algorithms intend to recover the degraded image from the remaining ambiguous content. In this case, the available features are limited, especially in hybrid conditions, and it is extremely challenging to recover high-quality images with insufficient information. Inspired by two-stage image generation models, which build a Code-

book with rich contexts in the first stage and then generate images with encoded discrete vectors in the second stage. We utilize the prior context-rich vectors embedded in the Codebook to assist the network in repairing degraded images, which allows the knowledge domain of restoration to be extended from a single image to the entire vectors repository. For the input feature map F_{mi} , the mapping network maps the features of the degraded image to the quantization encodings corresponding to the hidden clean image in Codebook, i.e., the reconstruction vectors. Benefiting from the information-rich image components contained in the reconstruction vectors, the restoration network can better reconstruct high-quality images.

More precisely, we utilize the VQGAN [11] pre-trained on OpenImages [20] with 8192 quantization encodings as a library of reconstruction vectors. The VQGAN encoder first produces the quantized encoding $F_{rv}^c \in \mathbb{R}^{\frac{H}{8} \times \frac{W}{8} \times N_z}$ of the clean image, and for the degraded image feature F_{mi} encoded by the restoration network encoder, the mapping network learns to predict the possible embedding F_{rv}^d that consistent with F_{rv}^c . Attention and convolution layers are cascaded to construct the mapping network which can be optimized by the following cosine similarity loss.

$$\mathcal{L}_{map} = \sum_{i=0}^{\frac{W}{8}} \sum_{j=0}^{\frac{H}{8}} \left[\frac{1 - \cos(F_{rv}^d(i, j), F_{rv}^c(i, j))}{\frac{W}{8} \times \frac{H}{8}} \right]. \quad (2)$$

We can then obtain F_{rv} by leveraging a subsequent nearest neighbor matching $NNM(\cdot)$ of each spatial encoding $F_{rv}^d(i, j) \in \mathbb{R}^{N_z}$ from $F_{rv}^c \in \mathbb{R}^{\frac{H}{8} \times \frac{W}{8} \times N_z}$ onto its closest reconstruction vector rv_k in the Codebook. The schematic illustration of this process is depicted in Fig. 2.

3.3. Output Space Discrimination

Existing all-in-one restoration approaches rely on distillation [8], degradation guidance [22], and querying [50] to gain knowledge of different degradations. Although these methods achieve excellent performance for non-overlapping degradation, they are limited in modeling the joint characterization of hybrid multiple degradations. Our intuition is that regardless of the degradation type image suffered, the restored result should be a degeneration-independent high-quality clean image. Thus, we innovatively treat the unified learning of multiple hybrid degradations as a domain adaptive problem and cultivate the degradation-independent adaptive restoration network via a discriminative adversarial learning scheme. In contrast to Li *et al.* [25] that strives to reserve degradation cues to train multiple feature extractors, we dedicate to back-constraining the restoration network to yield consistent degeneration-independent ideal images.

Discriminator Training. Given the restoration output $R = Network(D)$, we forward R to discriminator Dis to distinguish the type of weather degradation from the restored

image. The training of the discriminator can be regarded as a multilabel classification task, and the cross-entropy loss objective can be defined as:

$$\mathcal{L}_d = \sum_{i=0}^{n-1} [-t_i \log Dis(R)_i - (1 - t_i) \log(1 - Dis(R)_i)], \quad (3)$$

where n denotes the number of degenerate types, $t_i = 1$ if I suffer from degradation i else $t_i = 0$.

Restoration Network Training. First, pixel-level L1 loss is equipped to allow the restoration results R to approximate the ground truth clean image C :

$$\mathcal{L}_{net}^{l1} = \| R - C \|_1. \quad (4)$$

Second, to allow restoring degeneration-independent results, i.e., results that can not be recognized by the discriminator what degeneration types suffered, a discriminative loss is employed:

$$\mathcal{L}_{net}^{dis} = \sum_{i=0}^n -\log(1 - Dis(R)_i). \quad (5)$$

The ultimate goal is to minimize the L1 loss while allowing the results to approximate consistent degeneration-independent clean distribution. Meanwhile, perceptual loss \mathcal{L}_{net}^{per} [16] is also employed to weaken the interference of noise from pseudo-data on the training. Thus, the final training objective can be expressed as:

$$\mathcal{L}_{net} = \mathcal{L}_{net}^{l1} + \lambda_{dis} \mathcal{L}_{net}^{dis} + \mathcal{L}_{net}^{per}, \quad (6)$$

where λ_{dis} is set to 0.1 to balance relative weight of \mathcal{L}_{net}^{dis} .

The proposed paradigm can cope with 31 hybrid weather conditions by relying only on a five-class classification discriminator, whereas existing approaches have to treat 31 scenarios separately, resulting in a sophisticated and redundant training process.

3.4. Hybrid Adverse Weather Conditions Dataset

AdverseGAN for Training Set Generation. Pseudo-data generation [37, 70, 62, 55, 31, 64, 58] has been shown to be feasible and has achieved notable performance. Inspired by the above research, to efficiently generate realistic and controllable paired data for end-to-end training of arbitrary hybrid adverse conditions restoration, we propose to generate pseudo-adverse conditions with GAN rather than artificial processing. The key insight is to first train an elaborated AdverseGAN that can generate five basic weather types by leveraging existing data and then mixed-superposition conditions can be generated by recursive calls. Therefore, ultimately we can automatically generate 31 adverse conditions without manual operation. Schematic illustration of the proposed AdverseGAN is provided in Fig. 4.

Following recent works [60, 21, 1, 19], our generator is constructed based on a dual space structure, content space \mathcal{C} [1] and style space \mathcal{S} [18]. The generator first encodes the input clean image into a latent space and then generates the degraded image by injecting randomly drawn content

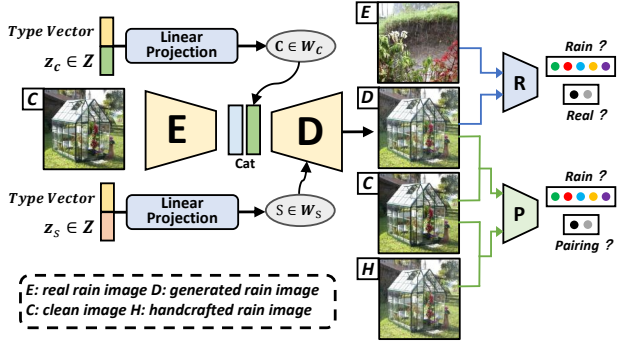


Figure 4. Pipeline of our proposed AdverseGAN. The generator is an encoder-decoder structure, consisting of two latent space injection branches: content branch (top) and style branch (bottom). And there are two discriminators: Realism-Discriminator (R) and Pairing-Discriminator (P).

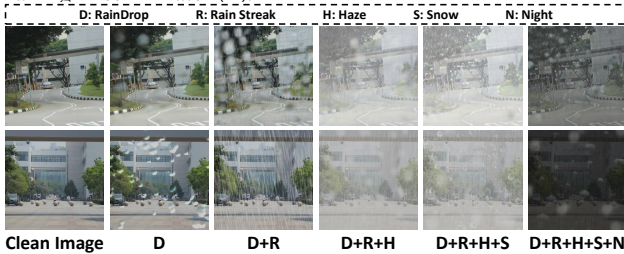


Figure 5. Top: Examples of training set images in HAC. Bottom: Examples of test set images in HAC. Best viewed at screen!

vector z_c and style vector z_s from a normal distribution. The type vector z_t , which maps from the type label t , is also integrated to control the condition type, similar to the conditional generative adversarial network (cGAN) [51].

While paired datasets of individual degradation types are readily available, most of them are synthetic and may not adequately simulate real-world degradation scenarios. Additionally, generative adversarial networks may not be able to maintain consistent backgrounds between generated images and their input versions. To address these limitations, we introduce a dual discriminator constraint regime. The realism-discriminator distinguishes between real-world adverse conditions and generated fake images, while the pairing-discriminator distinguishes between real and pseudo pairing data. To enable the generation of multiple adverse conditions, our discriminator produces probability distributions over both sources and condition types [36]. The dual discriminators work collaboratively to ensure that our proposed AdverseGAN generates realistic, content-preserved, and reliable adverse weather conditions. More details on AdverseGAN architecture and training setting can be found in the Suppl.

Handcrafted Test Set. Since the training set can be generated by AdverseGAN, to guarantee the authority and accuracy of evaluation, the test set is carefully fabricated artificially. We first capture 200 high-quality well-curated im-

ages (720×480) as ground truth with Canon EOS 60D, and then synthesize corresponding 31 adverse conditions for each image, resulting in 6200 image pairs. The synthesis of haze, rain streak, snow, night, and raindrop follows previous academic literature [23, 12, 30, 57, 43]. Photoshop-related works were performed by three photography experts we recruited. Lighting conditions, scenes, subjects, and styles, e.g., are all taken into account to ensure realism and diversity. Examples of HAC are illustrated in Fig. 5.

4. Experiments

4.1. Evaluation on HAC Dataset

The quantitative results on HAC dataset are reported in Tab. 1. As can be found, our RAHC delivers unparalleled performance gains and outperforms all competitive models both in the condition-specific setting and in the all-in-one setting, especially for extremely adverse scenarios such as “Quadruple” and “Pentuple”. Notably, RAHC exceeds the top-performing unified approach TKL [8] by 3.32dB on PSNR when there are pentuple degradation types. Furthermore, RAHC trained in the all-in-one setting even surpasses the results separately trained in each single condition. This phenomenon can be ascribed to the fact that the proposed discriminative learning scheme allows the network to learn more generalized and degradation-independent repair capabilities, and that the reconstruction vectors aided scheme can benefit from more sufficient data. We also demonstrate visual comparisons in Fig. 6. As suggested, RAHC recovers clean and crisp results while achieving a harmonious global tone without introducing visible artifacts or color shifts suffered by other methods, especially for complicated hybrid scenarios.

4.2. Evaluation on Conventional Datasets

Apart from our proposed HAC dataset, we also conduct experiments with SOTA algorithms on five conventional datasets in the all-in-one multi-weather removal setting. Tab. 2 shows that our RAHC yields consistent and significant performance gains over existing approaches on all five weather types. Compared to the recent best method TKL [8], our approach achieves 0.44 dB PSNR improvement when averaged across all test sets.

4.3. Ablation Study and Discussion

Effectiveness of MHBB. Fig. 7 provides the visualization of feature maps obtained from different heads in MHBB. It is observed that each head in MHBB provides a distinct representation subspace that performs its respective duties to characterize specific degradations under hybrid adverse weather conditions. By leveraging these representation subspaces, MHBB allows more flexibility to characterize the hybrid multiple weather degradations simultaneously.

Visual Evaluation of Reconstruction Vectors. We also

Table 1. Quantitative Comparison with the SOTA methods on our proposed benchmark HAC dataset. Top super row: single model instance for single condition (condition-specific). Bottom super row: one model instance for all conditions (all-in-one). Multiplicative numeral indicates the number of weather types contained in an image (e.g., Triple represents the average scores of $C_5^3 = 10$ conditions containing three weather types). Best and second best scores are **highlighted** and underlined.

Method	Single		Double		Triple		Quadruple		Pentuple		Average	
	PSNR	SSIM										
MIRNet [66]	28.44	0.9285	22.10	0.8749	19.11	0.7940	15.74	0.6483	14.30	0.6257	19.94	0.7743
HI-Net [5]	28.99	0.9393	23.33	0.9101	20.48	0.8422	16.14	0.6982	14.69	0.6689	20.73	0.8117
MPRNet [67]	28.84	0.9322	22.79	0.9147	20.19	0.8375	15.99	0.6858	14.65	0.6653	20.49	0.8071
SwinIR [26]	29.08	0.9411	24.21	0.9199	20.85	0.8517	16.78	0.7599	14.87	0.6672	21.16	0.8280
Uformer [56]	29.17	0.9425	24.48	0.9228	21.05	0.8533	16.89	0.7683	14.95	0.6728	21.31	0.8319
Restormer [65]	29.30	0.9478	24.60	0.9239	21.08	0.8531	16.92	0.7701	15.04	0.6783	21.39	0.8350
NAFNet [4]	29.35	0.9513	24.71	0.9276	21.12	0.8583	<u>17.01</u>	0.7864	<u>15.23</u>	0.6844	21.48	0.8416
RAHC	29.45	0.9517	24.98	0.9298	22.03	0.8817	19.53	0.8395	18.09	0.7502	22.82	0.8706
NAFNet [4]	29.10	0.9407	24.22	0.9143	20.74	0.8465	15.83	0.6623	14.33	0.6287	20.84	0.7985
TransWeather [50]	29.16	0.9433	24.25	0.9155	20.83	0.8495	16.72	0.7555	14.72	0.6652	21.14	0.8258
AirNet [22]	29.19	0.9436	24.32	0.9207	20.97	0.8522	16.87	0.7655	15.01	0.6741	21.27	0.8312
TKL [8]	29.23	0.9441	24.36	0.9229	21.05	0.8531	16.93	0.7725	14.92	0.6734	21.30	0.8332
RAHC	29.40	0.9514	24.91	0.9283	22.17	0.8946	19.88	0.8425	18.24	0.7612	22.92	0.8756



Figure 6. Visual comparisons with SOTA adverse conditions restoration methods on the HAC dataset. Reconstructed images demonstrate the ability of RAHC to restore arbitrary hybrid adverse conditions while preserving more details, hence yielding more visually pleasing results. **Best viewed at screen!**

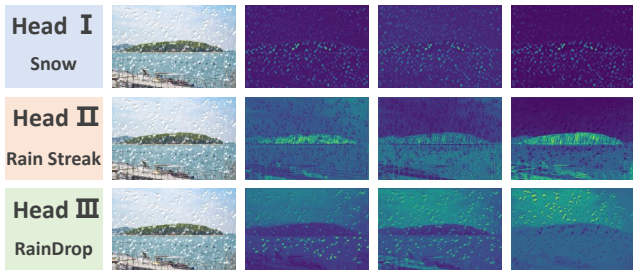


Figure 7. Visualization of feature maps from different heads in MHBB. The input image contains snow, rain streak and raindrop.

explored the visual effect of reconstruction vectors, and the results are provided in Fig. 8. As suggested, RAHC without RV tends to produce ambiguous contexts while our RAHC can restore sharper structural and textural details. Naturally, recovering clean images from the reconstruction vectors directly using the VQGAN decoder may be another option, but in this paper, we only leverage the reconstruction vectors as auxiliary features and let the network learn how to utilize them on its own. Such a strategy can also be demonstrated in Fig. 8. It is observed that the directly restored

images (Visual of RV) complement the possible textures of the degraded region but with low fidelity, while our implicit modeling allows the restoration model to use the visual atoms embedded in the reconstruction vector according to its own “experience”, hence restoring more realistic and reliable images with rich details.

Feature-Level Discrimination vs. Output Space Discrimination.

Analogous to the output space discrimination, we further investigate feature-level discrimination that is input the encoder-extracted features into the discriminator to distinguish the type of degradation. Quantitative experimental results are shown in Tab. 3, as can be found, both feature-level and output space contribute to learning degradation-independent restoration capacity while our output space is more favored compared to the counterparts. We conjecture that intermediate features containing high-level semantics are more prone to perplex the discriminator, which leads to weaker binding of the discriminator. Especially when performing discriminations at feature-level and output space simultaneously, the higher-level semantics can further disrupt the output space constraints.

Table 2. Quantitative Comparison with SOTA all-in-one multi-weather removal algorithms on five conventional datasets. Due to limited space, more adequate experimental results are given in the Suppl.

Method	Snow100K-L [30]		Raindrop [41]		SOTS-outdoor [23]		Rain1200 [68]		SICE [2]		Average	
	PSNR	SSIM	PSNR	SSIM	PSNR	SSIM	PSNR	SSIM	PSNR	SSIM	PSNR	SSIM
NAFNet [4]	30.32	0.8983	31.94	0.9291	29.87	0.9744	34.12	0.9561	20.16	0.6638	29.28	0.8843
TransWeather [50]	30.28	0.8987	31.74	0.9279	33.01	0.9768	34.05	0.9535	20.42	0.6973	29.90	0.8908
AirNet [22]	30.41	0.9087	32.27	0.9315	33.09	0.9808	34.19	0.9562	20.65	0.6993	30.12	0.8953
TKL [8]	<u>30.52</u>	<u>0.9098</u>	<u>32.35</u>	<u>0.9341</u>	<u>33.13</u>	<u>0.9792</u>	<u>34.25</u>	<u>0.9549</u>	<u>21.26</u>	<u>0.7131</u>	<u>30.30</u>	<u>0.8982</u>
RAHC	31.08	0.9115	32.82	0.9401	33.54	0.9865	34.71	0.9641	21.56	0.7269	30.74	0.9058

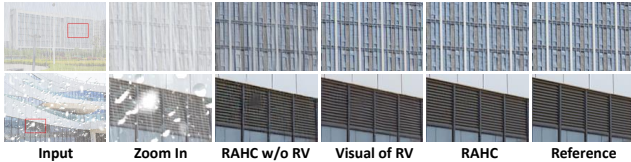


Figure 8. Visual effect of reconstruction vectors. Visualizations of reconstruction vectors were obtained by the VQGAN decoder. RV represents reconstruction vectors.

Variant	None	FL	FL + OS	OS (Ours)
PSNR	22.41	22.71	22.76	22.92

Table 4. Results of applying TKL strategy [8] proposed by Chen *et al.* (top rows) and output space discriminative learning scheme (OSD) proposed in this study (middle rows) into SOTA universal image restoration methods. Performance gains compared to pure training process are provided in parenthesis.

Method	PSNR	SSIM
Restormer [65] + TKL	21.14 (↑ 0.30)	0.8156 (↑ 0.0172)
NAFNet [4] + TKL	21.22 (↑ 0.38)	0.8215 (↑ 0.0230)
Restormer [65] + OSD	21.31 (↑ 0.47)	0.8301 (↑ 0.0317)
NAFNet [4] + OSD	21.37 (↑ 0.53)	0.8339 (↑ 0.0354)
TransWeather [50]	21.14	0.8258
AirNet [22]	21.27	0.8312
TKL [8]	21.30	0.8332
RAHC	22.92	0.8756

Universal Output Space Discrimination As mentioned above, our proposed OSD scheme can be integrated into existing universal image restoration architectures boosting their performance under all-in-one setting. Similarly, TKL [8] proposed by Chen *et al.* can also be applied to existing algorithms, and we have compared the superiority and inferiority of the two approaches under a fair backbone. As presented in Tab. 4, all algorithms show a significant performance improvement under the all-in-one setting when the OSD scheme is equipped which is more obvious and noticeable than the TKL strategy. In particular, Restormer [65] and NAFNet [4] even surpass the extant state-of-the-art unified framework TKL [8] with the original backbone in their paper and our mechanism is more flexible and straightforward compared to TKL’s multi-teacher distillation.

Reliability of AdverseGAN. Inevitably, the generated fake

Table 5. Comparison of training with original data (a) and AdverseGAN generated data. AdverseGAN can generate sufficient and reliable data with extremely cheap costs.

Sources	AirNet	TKL	RAHC	Time consuming
Original (a)	18.31	18.54	19.16	Approx. 1 month / person
AdverseGAN (c)	18.25	18.46	19.12	Approx. 10 minutes / GPU



Figure 9. Five examples of real-world adverse conditions restoration delivered by our RAHC. Best viewed at screen!

images would introduce undesired artifacts, which seems to compromise the training of the model, but we found the hazard of this to be minimal. To prove this, we randomly take 80% (a) from the test set of HAC for training and the remaining 20% (b) for testing. Then based on the clean images in (a), we utilize AdverseGAN to produce the generated data (c) in equal amounts with (a). We train the models on (a) and (c) separately and test them on (b). As shown in Tab. 5, the models trained on (c) achieve comparable performance to the one trained on (a), while the generated data are labor-effective and can produce infinite unduplicated data.

4.4. Visual Results on Real-World Conditions

Fig. 9 exhibits real-world adverse conditions restoration results by RAHC trained on the HAC dataset, the photo-realistic results demonstrate both the realistic reliability of HAC and the robustness of RAHC. Additionally, this experiment also reveals the truth that real-world scenarios often suffer from multiple superimposed degradations rather than simple one corruption, and our method can restore arbitrary hybrid conditions in one go.

5. Concluding Remarks

In this paper, we proposed a novel unified framework, namely RAHC to restore arbitrary hybrid adverse weather conditions in one go. In contrast to existing frameworks, RAHC can handle severely deteriorated scenarios suffered from hybrid weather degradations and restore arbitrary hybrid conditions with a single trained model by a concise and flexible scheme. Meanwhile, MHBB provides comprehensive degradation characterization and representation support. In addition, we propose a hybrid adverse conditions generation pipeline, based on which sufficient training data can be generated cost-effectively. And then finally established HAC dataset contains $\sim 316K$ image pairs of 31 types, which richness and diversity render it a competent evaluator. Extensive experiments on HAC and conventional datasets manifest the effectiveness, superiority, and robustness of our proposed RACH. We expect this work to provide insights into arbitrary hybrid adverse conditions restoration and steer future research on this Gordian knot.

References

- [1] Yazeed Alharbi and Peter Wonka. Disentangled image generation through structured noise injection. In *Proceedings of the IEEE/CVF Conference on Computer Vision and Pattern Recognition*, pages 5134–5142, 2020.
- [2] Jianrui Cai, Shuhang Gu, and Lei Zhang. Learning a deep single image contrast enhancer from multi-exposure images. *IEEE Transactions on Image Processing*, 27(4):2049–2062, 2018.
- [3] Nicolas Carion, Francisco Massa, Gabriel Synnaeve, Nicolas Usunier, Alexander Kirillov, and Sergey Zagoruyko. End-to-end object detection with transformers. In *European conference on computer vision*, pages 213–229. Springer, 2020.
- [4] Liangyu Chen, Xiaojie Chu, Xiangyu Zhang, and Jian Sun. Simple baselines for image restoration. *arXiv preprint arXiv:2204.04676*, 2022.
- [5] Liangyu Chen, Xin Lu, Jie Zhang, Xiaojie Chu, and Chengpeng Chen. Hinet: Half instance normalization network for image restoration. In *Proceedings of the IEEE/CVF Conference on Computer Vision and Pattern Recognition*, pages 182–192, 2021.
- [6] Liang-Chieh Chen, Yukun Zhu, George Papandreou, Florian Schroff, and Hartwig Adam. Encoder-decoder with atrous separable convolution for semantic image segmentation. In *Proceedings of the European conference on computer vision (ECCV)*, pages 801–818, 2018.
- [7] Wei-Ting Chen, Hao-Yu Fang, Cheng-Lin Hsieh, Cheng-Che Tsai, I Chen, Jian-Jiun Ding, Sy-Yen Kuo, et al. All snow removed: Single image desnowing algorithm using hierarchical dual-tree complex wavelet representation and contradict channel loss. In *Proceedings of the IEEE/CVF International Conference on Computer Vision*, pages 4196–4205, 2021.
- [8] Wei-Ting Chen, Zhi-Kai Huang, Cheng-Che Tsai, Hao-Hsiang Yang, Jian-Jiun Ding, and Sy-Yen Kuo. Learning multiple adverse weather removal via two-stage knowledge learning and multi-contrastive regularization: Toward a unified model. In *Proceedings of the IEEE/CVF Conference on Computer Vision and Pattern Recognition*, pages 17653–17662, 2022.
- [9] Marius Cordts, Mohamed Omran, Sebastian Ramos, Timo Rehfeld, Markus Enzweiler, Rodrigo Benenson, Uwe Franke, Stefan Roth, and Bernt Schiele. The cityscapes dataset for semantic urban scene understanding. In *Proceedings of the IEEE conference on computer vision and pattern recognition*, pages 3213–3223, 2016.
- [10] Hang Dong, Jinshan Pan, Lei Xiang, Zhe Hu, Xinyi Zhang, Fei Wang, and Ming-Hsuan Yang. Multi-scale boosted dehazing network with dense feature fusion. In *Proceedings of the IEEE/CVF conference on computer vision and pattern recognition*, pages 2157–2167, 2020.
- [11] Patrick Esser, Robin Rombach, and Bjorn Ommer. Taming transformers for high-resolution image synthesis. In *Proceedings of the IEEE/CVF conference on computer vision and pattern recognition*, pages 12873–12883, 2021.
- [12] Xueyang Fu, Jiabin Huang, Xinghao Ding, Yinghao Liao, and John Paisley. Clearing the skies: A deep network architecture for single-image rain removal. *IEEE Transactions on Image Processing*, 26(6):2944–2956, 2017.
- [13] Xueyang Fu, Jiabin Huang, Delu Zeng, Yue Huang, Xinghao Ding, and John Paisley. Removing rain from single images via a deep detail network. In *Proceedings of the IEEE conference on computer vision and pattern recognition*, pages 3855–3863, 2017.
- [14] Anmol Gulati, James Qin, Chung-Cheng Chiu, Niki Parmar, Yu Zhang, Jiahui Yu, Wei Han, Shibo Wang, Zhengdong Zhang, Yonghui Wu, et al. Conformer: Convolution-augmented transformer for speech recognition. *arXiv preprint arXiv:2005.08100*, 2020.
- [15] Judy Hoffman, Eric Tzeng, Taesung Park, Jun-Yan Zhu, Phillip Isola, Kate Saenko, Alexei Efros, and Trevor Darrell. Cycada: Cycle-consistent adversarial domain adaptation. In *International conference on machine learning*, pages 1989–1998. Pmlr, 2018.
- [16] Justin Johnson, Alexandre Alahi, and Li Fei-Fei. Perceptual losses for real-time style transfer and super-resolution. In *European conference on computer vision*, pages 694–711. Springer, 2016.
- [17] Guoliang Kang, Yunchao Wei, Yi Yang, Yueting Zhuang, and Alexander Hauptmann. Pixel-level cycle association: A new perspective for domain adaptive semantic segmentation. *Advances in Neural Information Processing Systems*, 33:3569–3580, 2020.
- [18] Tero Karras, Samuli Laine, Miika Aittala, Janne Hellsten, Jaakko Lehtinen, and Timo Aila. Analyzing and improving the image quality of stylegan. In *Proceedings of the IEEE/CVF conference on computer vision and pattern recognition*, pages 8110–8119, 2020.
- [19] Kunhee Kim, Sanghun Park, Eunyeong Jeon, Taehun Kim, and Daijin Kim. A style-aware discriminator for controllable image translation. In *Proceedings of the IEEE/CVF Conference on Computer Vision and Pattern Recognition*, pages 18239–18248, 2022.

- [20] Alina Kuznetsova, Hassan Rom, Neil Alldrin, Jasper Uijlings, Ivan Krasin, Jordi Pont-Tuset, Shahab Kamali, Stefan Popov, Matteo Mallocci, Alexander Kolesnikov, et al. The open images dataset v4. *International Journal of Computer Vision*, 128(7):1956–1981, 2020.
- [21] Gihyun Kwon and Jong Chul Ye. Diagonal attention and style-based gan for content-style disentanglement in image generation and translation. In *Proceedings of the IEEE/CVF International Conference on Computer Vision*, pages 13980–13989, 2021.
- [22] Boyun Li, Xiao Liu, Peng Hu, Zhongqin Wu, Jiancheng Lv, and Xi Peng. All-In-One Image Restoration for Unknown Corruption. In *Proceedings of the IEEE/CVF Conference on Computer Vision and Pattern Recognition*, pages 17452–17462, 2022.
- [23] Boyi Li, Wenqi Ren, Dengpan Fu, Dacheng Tao, Dan Feng, Wenjun Zeng, and Zhangyang Wang. Benchmarking single-image dehazing and beyond. *IEEE Transactions on Image Processing*, 28(1):492–505, 2018.
- [24] Ruoteng Li, Loong-Fah Cheong, and Robby T Tan. Heavy rain image restoration: Integrating physics model and conditional adversarial learning. In *Proceedings of the IEEE/CVF Conference on Computer Vision and Pattern Recognition*, pages 1633–1642, 2019.
- [25] Ruoteng Li, Robby T Tan, and Loong-Fah Cheong. All in one bad weather removal using architectural search. In *Proceedings of the IEEE/CVF conference on computer vision and pattern recognition*, pages 3175–3185, 2020.
- [26] Jingyun Liang, Jiezhong Cao, Guolei Sun, Kai Zhang, Luc Van Gool, and Radu Timofte. Swinir: Image restoration using swin transformer. In *Proceedings of the IEEE/CVF International Conference on Computer Vision*, pages 1833–1844, 2021.
- [27] Ming Liang, Bin Yang, Shenlong Wang, and Raquel Urtasun. Deep continuous fusion for multi-sensor 3d object detection. In *Proceedings of the European conference on computer vision (ECCV)*, pages 641–656, 2018.
- [28] Risheng Liu, Long Ma, Jiaao Zhang, Xin Fan, and Zhongxuan Luo. Retinex-inspired unrolling with cooperative prior architecture search for low-light image enhancement. In *Proceedings of the IEEE/CVF Conference on Computer Vision and Pattern Recognition*, pages 10561–10570, 2021.
- [29] Xiaohong Liu, Yongrui Ma, Zhihao Shi, and Jun Chen. Grid-dehazenet: Attention-based multi-scale network for image dehazing. In *Proceedings of the IEEE/CVF international conference on computer vision*, pages 7314–7323, 2019.
- [30] Yun-Fu Liu, Da-Wei Jaw, Shih-Chia Huang, and Jenq-Neng Hwang. Desnownet: Context-aware deep network for snow removal. *IEEE Transactions on Image Processing*, 27(6):3064–3073, 2018.
- [31] Zhihao Liu, Hui Yin, Xinyi Wu, Zhenyao Wu, Yang Mi, and Song Wang. From shadow generation to shadow removal. In *Proceedings of the IEEE/CVF Conference on Computer Vision and Pattern Recognition*, pages 4927–4936, 2021.
- [32] Jonathan Long, Evan Shelhamer, and Trevor Darrell. Fully convolutional networks for semantic segmentation. In *Proceedings of the IEEE conference on computer vision and pattern recognition*, pages 3431–3440, 2015.
- [33] Yawei Luo, Ping Liu, Liang Zheng, Tao Guan, Junqing Yu, and Yi Yang. Category-level adversarial adaptation for semantic segmentation using purified features. *IEEE Transactions on Pattern Analysis and Machine Intelligence*, 2021.
- [34] Yawei Luo, Liang Zheng, Tao Guan, Junqing Yu, and Yi Yang. Taking a closer look at domain shift: Category-level adversaries for semantics consistent domain adaptation. In *Proceedings of the IEEE/CVF Conference on Computer Vision and Pattern Recognition*, pages 2507–2516, 2019.
- [35] Zak Murez, Soheil Kolouri, David Kriegman, Ravi Ramamoorthi, and Kyungnam Kim. Image to image translation for domain adaptation. In *Proceedings of the IEEE Conference on Computer Vision and Pattern Recognition*, pages 4500–4509, 2018.
- [36] Augustus Odena, Christopher Olah, and Jonathon Shlens. Conditional image synthesis with auxiliary classifier gans. In *International conference on machine learning*, pages 2642–2651. PMLR, 2017.
- [37] Xingang Pan, Ayush Tewari, Lingjie Liu, and Christian Theobalt. Gan2x: Non-lambertian inverse rendering of image gans. *arXiv preprint arXiv:2206.09244*, 2022.
- [38] Asanka G Perera, Yee Wei Law, and Javaan Chahl. Uav-gesture: A dataset for uav control and gesture recognition. In *Proceedings of the European Conference on Computer Vision (ECCV) Workshops*, pages 0–0, 2018.
- [39] Aditya Prakash, Kashyap Chitta, and Andreas Geiger. Multi-modal fusion transformer for end-to-end autonomous driving. In *Proceedings of the IEEE/CVF Conference on Computer Vision and Pattern Recognition*, pages 7077–7087, 2021.
- [40] Charles R Qi, Wei Liu, Chenxia Wu, Hao Su, and Leonidas J Guibas. Frustum pointnets for 3d object detection from rgb-d data. In *Proceedings of the IEEE conference on computer vision and pattern recognition*, pages 918–927, 2018.
- [41] Rui Qian, Robby T Tan, Wenhan Yang, Jiajun Su, and Jiaying Liu. Attentive generative adversarial network for rain-drop removal from a single image. In *Proceedings of the IEEE conference on computer vision and pattern recognition*, pages 2482–2491, 2018.
- [42] Xu Qin, Zhilin Wang, Yuanchao Bai, Xiaodong Xie, and Huizhu Jia. Ffa-net: Feature fusion attention network for single image dehazing. In *Proceedings of the AAAI Conference on Artificial Intelligence*, volume 34, pages 11908–11915, 2020.
- [43] Ruijie Quan, Xin Yu, Yuanzhi Liang, and Yi Yang. Removing raindrops and rain streaks in one go. In *Proceedings of the IEEE/CVF Conference on Computer Vision and Pattern Recognition*, pages 9147–9156, 2021.
- [44] Yuhui Quan, Shijie Deng, Yixin Chen, and Hui Ji. Deep learning for seeing through window with raindrops. In *Proceedings of the IEEE/CVF International Conference on Computer Vision*, pages 2463–2471, 2019.
- [45] Ali Razavi, Aaron Van den Oord, and Oriol Vinyals. Generating diverse high-fidelity images with vq-vae-2. *Advances in neural information processing systems*, 32, 2019.
- [46] Robin Rombach, Andreas Blattmann, Dominik Lorenz, Patrick Esser, and Björn Ommer. High-resolution image

- synthesis with latent diffusion models. In *Proceedings of the IEEE/CVF Conference on Computer Vision and Pattern Recognition*, pages 10684–10695, 2022.
- [47] Wenzhe Shi, Jose Caballero, Ferenc Huszár, Johannes Totz, Andrew P Aitken, Rob Bishop, Daniel Rueckert, and Zehan Wang. Real-time single image and video super-resolution using an efficient sub-pixel convolutional neural network. In *Proceedings of the IEEE conference on computer vision and pattern recognition*, pages 1874–1883, 2016.
- [48] Yuda Song, Zhuqing He, Hui Qian, and Xin Du. Vision transformers for single image dehazing. *arXiv preprint arXiv:2204.03883*, 2022.
- [49] Yi-Hsuan Tsai, Wei-Chih Hung, Samuel Schulter, Kihyuk Sohn, Ming-Hsuan Yang, and Manmohan Chandraker. Learning to adapt structured output space for semantic segmentation. In *Proceedings of the IEEE conference on computer vision and pattern recognition*, pages 7472–7481, 2018.
- [50] Jeya Maria Jose Valanarasu, Rajeev Yasarla, and Vishal M Patel. Transweather: Transformer-based restoration of images degraded by adverse weather conditions. In *Proceedings of the IEEE/CVF Conference on Computer Vision and Pattern Recognition*, pages 2353–2363, 2022.
- [51] Aaron Van den Oord, Nal Kalchbrenner, Lasse Espeholt, Oriol Vinyals, Alex Graves, et al. Conditional image generation with pixellcn decoders. *Advances in neural information processing systems*, 29, 2016.
- [52] Ashish Vaswani, Noam Shazeer, Niki Parmar, Jakob Uszkoreit, Llion Jones, Aidan N Gomez, Łukasz Kaiser, and Illia Polosukhin. Attention is all you need. *Advances in neural information processing systems*, 30, 2017.
- [53] Yecong Wan, Yuanshuo Cheng, Mingwen Shao, and Jordi González. Image rain removal and illumination enhancement done in one go. *Knowledge-Based Systems*, page 109244, 2022.
- [54] Hong Wang, Qi Xie, Qian Zhao, and Deyu Meng. A model-driven deep neural network for single image rain removal. In *Proceedings of the IEEE/CVF Conference on Computer Vision and Pattern Recognition*, pages 3103–3112, 2020.
- [55] Hong Wang, Zongsheng Yue, Qi Xie, Qian Zhao, Yefeng Zheng, and Deyu Meng. From rain generation to rain removal. In *Proceedings of the IEEE/CVF Conference on Computer Vision and Pattern Recognition*, pages 14791–14801, 2021.
- [56] Zhendong Wang, Xiaodong Cun, Jianmin Bao, Wengang Zhou, Jianzhuang Liu, and Houqiang Li. Uformer: A general u-shaped transformer for image restoration. In *Proceedings of the IEEE/CVF Conference on Computer Vision and Pattern Recognition*, pages 17683–17693, 2022.
- [57] Chen Wei, Wenjing Wang, Wenhan Yang, and Jiaying Liu. Deep retinex decomposition for low-light enhancement. *arXiv preprint arXiv:1808.04560*, 2018.
- [58] Yanyan Wei, Zhao Zhang, Yang Wang, Mingliang Xu, Yi Yang, Shuicheng Yan, and Meng Wang. Deraincyclegan: Rain attentive cyclegan for single image deraining and rain-making. *IEEE Transactions on Image Processing*, 30:4788–4801, 2021.
- [59] Haiyan Wu, Yanyun Qu, Shaohui Lin, Jian Zhou, Ruizhi Qiao, Zhizhong Zhang, Yuan Xie, and Lizhuang Ma. Contrastive learning for compact single image dehazing. In *Proceedings of the IEEE/CVF Conference on Computer Vision and Pattern Recognition*, pages 10551–10560, 2021.
- [60] Yanbo Xu, Yueqin Yin, Liming Jiang, Qianyi Wu, Chengyao Zheng, Chen Change Loy, Bo Dai, and Wayne Wu. Transeditor: Transformer-based dual-space gan for highly controllable facial editing. In *Proceedings of the IEEE/CVF Conference on Computer Vision and Pattern Recognition*, pages 7683–7692, 2022.
- [61] Wilson Yan, Yunzhi Zhang, Pieter Abbeel, and Aravind Srinivas. Videogpt: Video generation using vq-vae and transformers. *arXiv preprint arXiv:2104.10157*, 2021.
- [62] Zhenpei Yang, Yuning Chai, Dragomir Anguelov, Yin Zhou, Pei Sun, Dumitru Erhan, Sean Rafferty, and Henrik Kretschmar. Surfelgan: Synthesizing realistic sensor data for autonomous driving. In *Proceedings of the IEEE/CVF Conference on Computer Vision and Pattern Recognition*, pages 11118–11127, 2020.
- [63] Jiahui Yu, Xin Li, Jing Yu Koh, Han Zhang, Ruoming Pang, James Qin, Alexander Ku, Yuanzhong Xu, Jason Baldridge, and Yonghui Wu. Vector-quantized image modeling with improved vqgan. *arXiv preprint arXiv:2110.04627*, 2021.
- [64] Zongsheng Yue, Qian Zhao, Lei Zhang, and Deyu Meng. Dual adversarial network: Toward real-world noise removal and noise generation. In *European Conference on Computer Vision*, pages 41–58. Springer, 2020.
- [65] Syed Waqas Zamir, Aditya Arora, Salman Khan, Munawar Hayat, Fahad Shahbaz Khan, and Ming-Hsuan Yang. Restormer: Efficient transformer for high-resolution image restoration. In *Proceedings of the IEEE/CVF Conference on Computer Vision and Pattern Recognition*, pages 5728–5739, 2022.
- [66] Syed Waqas Zamir, Aditya Arora, Salman Khan, Munawar Hayat, Fahad Shahbaz Khan, Ming-Hsuan Yang, and Ling Shao. Learning enriched features for real image restoration and enhancement. In *European Conference on Computer Vision*, pages 492–511. Springer, 2020.
- [67] Syed Waqas Zamir, Aditya Arora, Salman Khan, Munawar Hayat, Fahad Shahbaz Khan, Ming-Hsuan Yang, and Ling Shao. Multi-stage progressive image restoration. In *Proceedings of the IEEE/CVF conference on computer vision and pattern recognition*, pages 14821–14831, 2021.
- [68] He Zhang and Vishal M Patel. Density-aware single image de-raining using a multi-stream dense network. In *Proceedings of the IEEE conference on computer vision and pattern recognition*, pages 695–704, 2018.
- [69] Kai Zhang, Yawei Li, Jingyun Liang, Jiezhang Cao, Yulun Zhang, Hao Tang, Radu Timofte, and Luc Van Gool. Practical blind denoising via swin-conv-unet and data synthesis. *arXiv preprint arXiv:2203.13278*, 2022.
- [70] Yuxuan Zhang, Huan Ling, Jun Gao, Kangxue Yin, Jean-Francois Lafleche, Adela Barriuso, Antonio Torralba, and Sanja Fidler. Datasetgan: Efficient labeled data factory with minimal human effort. In *Proceedings of the IEEE/CVF Conference on Computer Vision and Pattern Recognition*, pages 10145–10155, 2021.

- [71] Yonghua Zhang, Jiawan Zhang, and Xiaojie Guo. Kindling the darkness: A practical low-light image enhancer. In *Proceedings of the 27th ACM international conference on multimedia*, pages 1632–1640, 2019.
- [72] Jun-Yan Zhu, Taesung Park, Phillip Isola, and Alexei A Efros. Unpaired image-to-image translation using cycle-consistent adversarial networks. In *Proceedings of the IEEE international conference on computer vision*, pages 2223–2232, 2017.
- [73] Yang Zou, Zhiding Yu, BVK Kumar, and Jinsong Wang. Unsupervised domain adaptation for semantic segmentation via class-balanced self-training. In *Proceedings of the European conference on computer vision (ECCV)*, pages 289–305, 2018.